Investigation of shear banding in three-dimensional foams

Guillaume Ovarlez, Kapil Krishan, Sylvie Cohen-Addad

Investigation of shear banding in three-dimensional foams

G. Ovarlez[1], K. Krishan[2,3] and S. Cohen-Addad[3]

[1] *Université Paris-Est, Laboratoire Navier (UMR 8205 ENPC/LCPC/CNRS), 2 Allée Kepler, 77420 Champs-sur-Marne, France*
[2] *School of Physical Sciences, Jawaharlal Nehru University, New Delhi - 110067, India*
[3] *Université Paris-Est, Laboratoire de Physique des Matériaux Divisés et des Interfaces (FRE3300 CNRS), 5 Bd Descartes, Champs-sur-Marne, 77454 Marne-la-Vallée Cédex 2, France*

PACS 83.80.Iz – Emulsions and foams
PACS 83.10.Gr – Constitutive relations

Abstract. - We study the steady flow properties of different three-dimensional aqueous foams in a wide gap Couette geometry. From local velocity measurements through Magnetic Resonance Imaging techniques and from viscosity bifurcation experiments, we find that these foams do not exhibit any observable signature of shear banding. This contrasts with two previous results (Rodts *et al.*, *Europhys. Lett.*, **69** (2005) 636 and Da Cruz *et al.*, *Phys. Rev. E*, **66** (2002) 051305); we discuss possible reasons for this dicrepancy. Moreover, the foams we studied undergo steady flow for shear rates well below the critical shear rate recently predicted (Denkov *et al.*, *Phys. Rev. Lett.*, **103** (2009) 118302). Local measurements of the constitutive law finally show that these foams behave as simple Herschel-Bulkley yield stress fluids.

Introduction – Materials such as dense suspensions, colloidal gels, concentrated emulsions, foams or granular materials, present a jammed structure [1]. This results in the existence of a yield stress τ_y below which they cannot flow. It was recently shown that some of these materials exhibit shear banding while others do not [2–4]. Shear banding means that in some conditions (near τ_y), in a homogeneous shear stress field, there is coexistence of liquid (sheared) and solid (unsheared) regions [3,5,6]. At the interface between both regions, the material flows at a non-zero critical shear rate[1] $\dot{\gamma}_c$. This implies that shear banding materials cannot flow steadily at a shear rate smaller than $\dot{\gamma}_c$. If one shears such systems between two boundaries at a low macroscopic shear rate $\dot{\gamma}_{macro} < \dot{\gamma}_c$, local velocity measurements [7] then reveal shear banding [3]: the material splits into a region flowing at $\dot{\gamma}_c$ and a non flowing region, whose relative extent ensures that the shear rate spatial average is equal to $\dot{\gamma}_{macro}$. In macroscopic rheometric experiments, under applied stress, this leads to the viscosity bifurcation phenomenon [8,9]. This implies that, in addition to their yield stress, shear banding materials are also characterized by a critical shear rate $\dot{\gamma}_c$, thus defining a timescale which must have its origin at a microscopic scale. Therefore, two different classes of jammed systems should be considered depending on whether they exhibit shear banding or not. To understand the physical origin of this phenomenon, it is thus of high importance to identify which materials do exhibit shear banding and which do not.

Shear banding of jammed systems is observed mostly in colloidal gels [5,6,10], where aggregation due to attractive interactions and thermally activated structuration mechanisms is in competition with shear. It is also observed in suspensions of noncolloidal particles where it results from competition between sedimentation-induced contact formation (which can be seen as an attractive force) and shear-induced resuspension [11]. Some yield stress fluids seem not to exhibit shear banding, although experiments only provide upper bounds on $\dot{\gamma}_c$: neutrally buoyant noncolloidal suspensions [11], Carbopol gels [12], dense emulsions [13]. In all these cases, if a critical shear rate exists, it should be smaller than 10^{-2} s^{-1}. Hence, it is suggested that attractive, thixotropic systems tend to develop shear banding whereas repulsive and non-thermal systems do not [3, 10, 12].

In this context, the case of foams is rather puzzling. Disordered foams and dense emulsions are both soft jammed

[1]The situation is different in heterogeneous stress fields where shear localization occurs with any yield stress fluid. The shear rate at the interface between the sheared and unsheared regions is then naught for simple, non shear banding, yield stress fluids, whereas it is non-zero for shear banding materials [3].

packings of two immiscible fluids with similar structures and mechanical behaviors [14]. Their solid-like properties arise from their density of interfacial energy, and steady flow is accomplished by shear-induced structural rearrangements. Therefore, one could *a priori* expect foams to behave like emulsions with respect to shear banding. Shear banding in emulsions was reported once by Bécu *et al.* [15] but this result was later contradicted by Ovarlez *et al.* [13] who found $\dot{\gamma}_c < 10^{-2}$ s^{-1} for several emulsions. It is now believed that the shear bands observed in [15] are transient shear bands (as observed in Carbopol gels [16]), which disappear in steady state. Several cases of shear banding in 2D and 3D foams have been reported in the literature. Many observations of shear banding in 2D foams are now attributed to viscous damping at the glass boundary [17–20] when the bubbles are confined by one (or two) glass plate. The case of bubble rafts is still unclear. On the one hand, Gilbreth *et al.* [21] have reported a consistent set of shear banded velocity profiles characterized by a unique $\dot{\gamma}_c$; these profiles are claimed to be consistent with a single continuum model in a 10 to 20 bubbles-wide zone, although no stress measurement is reported. On the other hand, Katgert *et al.* [20] do not observe any signature of shear banding for rafts of equivalent bubble size to gap ratios. Moreover their velocity profiles are not consistent with a single constitutive law, but can be described by a non-local model, such as what is found in confined emulsions [22].

The only measurement of local bulk velocity profile we are aware of in steadily sheared 3D foams was performed by Rodts *et al.* [23] and revealed strong shear banding. Velocity profiles were measured by MRI in a wet foam (gas volume fraction $\phi = 92\%$) sheared in a Couette geometry. At low rotational velocity of the inner cylinder, flow localization was observed with a discontinuity of the shear rate at the interface between the sheared and the unsheared regions, thus providing a critical shear rate $\dot{\gamma}_c \simeq 5$ s^{-1}. Consistently, macroscopic strain rate measurements by Da Cruz *et al.* [9] in a similar 3D foam sheared in a homogeneous stress field (cone and plate geometry) showed a viscosity bifurcation, characterized by a critical shear rate $\dot{\gamma}_c \simeq 10$ s^{-1}.

To account for the observed shear banding in 3D foams and predict the value of $\dot{\gamma}_c$, Denkov *et al.* have proposed a model based on the thinning dynamics of the films between bubbles [24]. Shear flow induces rearrangements thus renewing bubble contacts. New films thin due to the capillary pressure set by the curvature of the Plateau borders. As their thickness reaches the range of van der Waals interactions, the film may thin abruptly to a Newton black film (of a few nm thickness) providing a strong adhesion between the bubbles and locally jamming the bubble packing. A critical shear rate then results from the competition between the timescale of shear-induced rearrangements and that of the Newton black film formation. It reads:

$$\dot{\gamma}_c = 1.9 \frac{T^{3/7} A_H^{4/7}}{\eta \langle d \rangle^{15/7} (1-\phi)^{0.3}} \qquad (1)$$

with A_H the Hamaker constant ($A_H \simeq 4\,10^{-20}$ J), T the surface tension, η the viscosity of the solution, and $\langle d \rangle$ the average bubble diameter. For a given ϕ, $\dot{\gamma}_c$ does not vary much with T and exhibits a marked dependency with η and $\langle d \rangle$. For instance, the value of $\dot{\gamma}_c$ expected for a typical Gillette foam is 10 s^{-1} (with T=28.6 mN/m, η= 1.9 mPas, ϕ=92% and $\langle d \rangle$= 40 μm). This prediction (see Fig. 1c) seems to be in good agreement with MRI data [23] and with recent qualitative measurements [24].

Finally, these results tend to show that 3D foams are not simple yield stress fluids, in contrast with dense emulsions. However, whereas solely local measurements of bulk velocity profiles can unambiguously determine the existence of steady shear banding in 3D foams, only one such measurement exists in the literature [23]. In this letter, we present a set of new experiments in 3D foams, with different gas volume fractions, bubble size and interfacial rheological properties. Local velocity profiles measured using MRI show that, in contrast with [9, 23], 3D foams do not exhibit any observable shear banding. Consistently, they do not exhibit viscosity bifurcation. They appear to behave as simple Herschel-Bulkley fluids, as previously found in emulsions [13].

Materials and methods – We study a foam based on a mixed surfactant aqueous solution, denoted SLES. It contains Sodium Lauryl-dioxyethylene Sulfate (Stepan Co., USA) with concentration 0.33% g/g, Cocoamidopropyl Betaine (Goldschmidt, Germany) with concentration 0.17% g/g and 60% g/g Glycerol (Fluka, anhydrous p.a. 99.5% GC). The chemicals are dissolved in water (millipore milli-Q). The surface tension and the viscosity of this solution at 21 ± 1 °C are $T = 31.0$ mN/m and $\eta = 10.8$ mPa s [25]. Foam is produced by simultaneously flowing the SLES solution and pressurized nitrogen gas saturated with perfluorohexane vapor through a glass bead column [26]. By adjusting the liquid flow rate and gas pressure, we produce samples with different controlled gas volume fractions ϕ. Using videomicroscopy, we characterize the average $\langle d \rangle$ of the bubble diameter d distribution and its dimensionless standard deviation $\mu = \sqrt{\langle d^2 \rangle - \langle d \rangle^2} / \langle d \rangle$ for each foam sample. We prepare three materials with same $\langle d \rangle = 73\,\mu$m (and μ comprised between 0.5 and 0.6), of different ϕ: (i) (88.4 ± 0.3)%, (ii) (92.5 ± 0.3)% , and (iii) (95.3 ± 0.3)%. In addition, we have a sample with $\langle d \rangle = 45\,\mu$m, $\mu = 0.7$, and $\phi = (92.5 \pm 0.3)$%. We also use Gillette shaving cream (Normal Regular), denoted Gillette NR, as in previous studies [27] for the sake of comparison with [9], with $\phi = (92.0 \pm 0.5)$%, $\langle d \rangle = 41\,\mu$m and $\mu = 0.6$. Its constitutive foaming solution has T = 28.6 mN/m and $\eta = 1.9$ mPa s [25]. For the sake of comparison with [23], we use another Gillette shaving cream (Haute Protection) denoted Gillette HP. As the rigidity of the liquid-gas in-

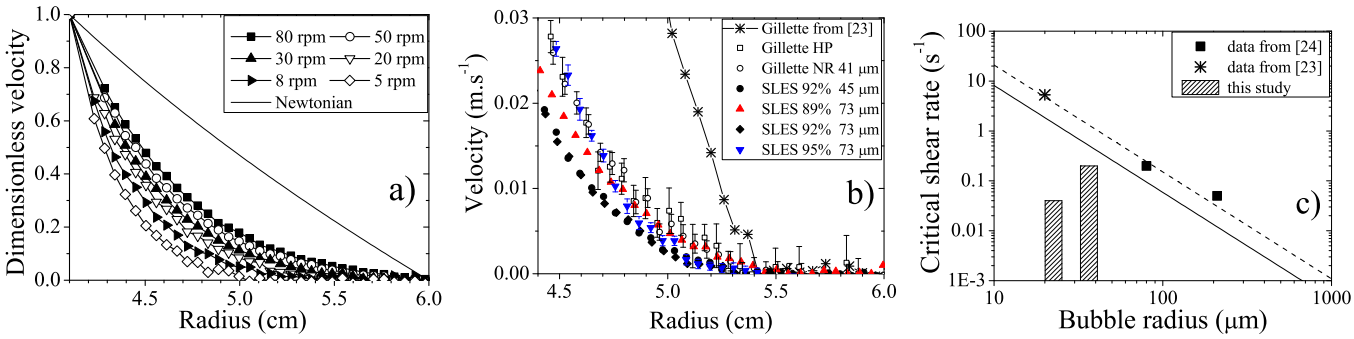

Fig. 1: a) Dimensionless velocity profiles $V(R)/V(R_i)$ for the steady flows of SLES foam ($\phi = 92\%$, $\langle d \rangle = 45$ μm), at various rotational velocities ranging from 5 to 80 rpm; the solid line is the theoretical profile for a Newtonian fluid. b) Comparison between localized velocity profiles of the foams we studied and that of Rodts *et al.* [23] (see ϕ and $\langle d \rangle$ in legend). c) Critical shear rate vs. bubble radius for foams with ϕ = 92-93%: Denkov *et al.* data [24] (squares), Rodts *et al.* data [23] (star); the hatched bars show the intervals of possible critical shear rates – if any – for the SLES foams in this study; the lines are Eq. 1 with $A_H = 4\,10^{-20}$ J (dashed line: $T = 22.3$ mN/m, $\phi = 93\%$, $\eta = 3.8$ mPa s; solid line: $T = 31.0$ mN/m, $\phi = 92\%$, $\eta = 10.8$ mPa s).

terfaces plays a role on the behavior of steadily sheared foams [28], it is interesting to test the influence of this parameter on shear banding. This can be done from our experiments (at $\phi = 92\%$ and $\langle d \rangle \simeq 40\mu$m) since in contrast to SLES foam, Gillette NR foam has rigid liquid-gas interfaces [25, 28].

The material's local behavior is studied in a wide-gap Couette geometry (inner cylinder radius R_i=4.1 cm; outer cylinder radius R_o=6 cm; height H=11 cm). The use of a wide gap likely prevents (non-local) finite size effects [13, 20, 22]. Sandpaper is glued to the walls to avoid slippage; there is no observable slip in the velocity profiles. The rheometer is inserted in a 0.5-T vertical MRI spectrometer (24/80 DBX by Bruker). In all experiments, the velocity Ω of the inner cylinder is controlled. We measure the local velocity in the flowing sample for various constant Ω ranging from 5 to 100 rpm; the torque exerted by the material on the inner cylinder is measured using a Bohlin C-VOR 200 rheometer. The orthoradial velocity profiles $V_\theta(R)$ are obtained through MRI techniques as described in [29,30]. The MRI setup also allows measurement of the local water content [30]. In all experiments, we checked that drainage can be neglected (it led to absolute volume fraction variations of order 0.5% in the 4cm high measurement zone over the duration of the experiments). We also checked that there is no observable shear-induced radial migration of water, as in emulsions [13].

As a complement and to allow for a direct comparison of our data with previous ones [9], we have performed macroscopic viscosity bifurcation experiments. Such macroscopic experiments are convincing only if the stress field is homogeneous; we thus use a 4° cone and plate geometry (as in [9]), with serrated surfaces of 30 mm radius; the stress heterogeneity is then of the order of 0.5%. Note however that the gap is small (the gap at the edge is 50 bubbles high); therefore, one cannot exclude finite size (non-local) effects [20,22]. Experiments consist in first applying a preshear at high shear rate (20 s^{-1}) during 60 s, ensuring that the whole material flows initially, before applying a constant stress for 150 to 300 s. The macroscopic shear rate is then plotted vs. time to check for the existence of a steady flow.

Velocity profiles and shear banding – In this section, we focus on the stationary velocity profiles. In Fig. 1a, we plot the dimensionless velocity profiles $V(R)/V(R_i)$ obtained with SLES foam ($\phi = 92\%$) for various rotational velocities Ω. All the studied foams exhibit similar behavior. We observe that the material is sheared only in a fraction of the gap at low Ω: $V(R)$ vanishes (within the measurement uncertainty) at some radius $R_c(\Omega) < R_o$. R_c increases with Ω. Beyond a critical velocity (that depends on the foam and is of order 40 rpm in Fig. 1a), the whole sample is sheared.

To analyze these observations, one should first be reminded that the shear stress distribution $\tau(R)$ is heterogeneous: it decreases with increasing radius R and reads $\tau(R) = \tau(R_i)\, R_i^2/R^2$ from stress balance equations. When shear extends over the whole gap, the velocity profiles differ from those of a Newtonian fluid. Their strong curvature is due to the stress heterogeneity (since $\tau(R_i)/\tau(R_o) = 2.1$) and is typical of shear-thinning fluid: the shear rate decreases more rapidly within the gap (*i.e.* when τ decreases) than for a Newtonian fluid. The shear localization observed at low velocity is a feature of yield stress fluid flow in Couette geometry. At low Ω (or applied stress slightly above the material yield stress τ_y), the flow stops at a radius R_c within the gap where the local shear stress $\tau(R)$ equals τ_y (*i.e.* $R_c = R_i\sqrt{\tau(R_i)/\tau_y}$). The decrease of $R_c(\Omega)$ as Ω is decreased then comes from the rate dependence of the constitutive law at the approach of τ_y. Note the discrepancy between this observation and that of Katgert *et al.* in 2D foams [20] where dimensionless ve-

locity profiles superpose and extend over the whole gap at any low Ω. We will discuss this differences in the section devoted to the constitutive law measurements.

From the shear localized velocity profiles, we now analyze the possible shear banding behavior of the studied foams. Two cases should be considered. On the one hand, if the material is a shear banding material, the shear rate $\dot{\gamma}(R)$ should tend towards a critical shear rate $\dot{\gamma}_c \neq 0$ as τ approaches τ_y *i.e.* as R tends to R_c. As $\dot{\gamma}(R) = V/R - \mathrm{d}V/\mathrm{d}R$, the local velocity should tend to zero with a non-zero slope $|\mathrm{d}V/\mathrm{d}R| = \dot{\gamma}_c$, independent of the velocity at the inner cylinder. Shear banding should then result in a discontinuity of the slope of the velocity profile at the interface between the sheared and the unsheared regions, as in a homogeneous stress field [3]. This is precisely as observed by Rodts *et al.* [23] (see Fig. 1b). For various Ω, they found a consistent set of shear banded velocity profiles with a slope $\dot{\gamma}_c \approx 5$ s^{-1} at the interface. On the other hand, if the material is not a shear banding material, $\dot{\gamma}(R)$ should tend continuously to zero as τ approaches τ_y *i.e.* as R tends to R_c. This would mean that $\mathrm{d}V/\mathrm{d}R = 0$ at the interface between the sheared and the unsheared regions *i.e.* the velocity profile should tend smoothly to zero.

In Fig. 1b, we plot shear localized velocity profiles obtained by Rodts *et al.* and by us corresponding to a same position of R_c (here $\simeq 5.4$ cm). We focus on the shape of the velocity profiles at the interface between the sheared and the unsheared regions. From this plot, it is clear that, in contrast with the Rodts *et al.* data, all of our systems exhibit a smooth transition from flow to rest and thus seem to be not shear banding materials. Of course, due to finite experimental resolution, we can never be certain that no critical shear rate exists. We can only provide upper bounds on the critical shear rate – if any – as shown in Tab. 1. Note that the accuracy of the shear rate measurement depends on the spatial resolution and on the MRI signal to noise ratio, which depends itself on the foaming solution and on external factors. The best experimental conditions were met with the 92% SLES foam, and led to a rather low upper bound ≈ 0.04 s^{-1}.

Foam	ϕ	$\langle d \rangle$	Upper bound on $\dot{\gamma}_c$	Model (Eq. 1)
SLES	92%	45 μm	0.04 s^{-1}	1.5 s^{-1}
SLES	88%	73 μm	0.2 s^{-1}	0.45 s^{-1}
SLES	92%	73 μm	0.2 s^{-1}	0.52 s^{-1}
SLES	95%	73 μm	0.3 s^{-1}	0.60 s^{-1}
Gillette NR	92%	41 μm	0.2 s^{-1}	9.6 s^{-1}
Gillette HP	–	–	0.6 s^{-1}	–

Table 1: Upper bounds on the critical shear rate $\dot{\gamma}_c$ obtained from MRI measurements and predictions of Eq. 1 for all foams.

Viscosity bifurcation – It is striking that we find upper bounds much lower than the critical shear rates $\dot{\gamma}_c$ previously reported [9, 23]. From macroscopic measurements, Da Cruz *et al.* evidenced a viscosity bifurcation in the Gillette NR foam [9], with $\dot{\gamma}_c \approx 10$ s^{-1}. To understand if viscosity bifurcation experiments can be reconciled with our local measurements, we have performed these experiments on some of our systems, including the Gillette NR foam of [9]. We focus on measurements obtained for applied stress close to the yield stress to estimate the lowest steady state shear rates than can be achieved.

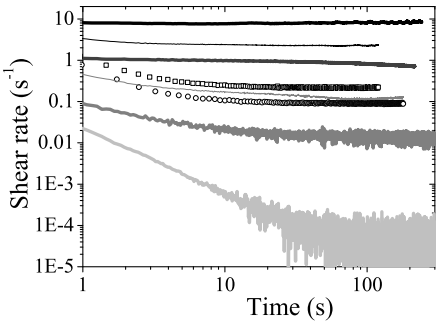

Fig. 2: Viscosity bifurcation experiments: shear rate vs. time at constant controlled stress in a cone and plate geometry. Thick lines: SLES foam with $\phi = 92\%$ and $\langle d \rangle = 45\mu$m (in grey scale, from black to light grey: 65 Pa, 45 Pa, 30 Pa, 20 Pa). Thin lines: Gillette HP as in [23] (black: 60 Pa, grey: 35 Pa). Empty symbols: Gillette NR as in [9], with $\langle d \rangle = 30\mu$m (squares: 60 Pa, circles: 50 Pa).

Fig. 2 shows that steady state flow can be achieved under controlled stress conditions at shear rate values as low as 0.1 s^{-1} for the two Gillette foams and 0.02 s^{-1} for the SLES foam. Further experiments would have to be performed to improve the estimate of the upper bound of $\dot{\gamma}_c$ from these indirect measurements. At this stage, the conclusion is that local and macroscopic measurements are consistent, and lead to the same result: the absence of observable shear banding in all foams we studied.

Analysis – We now question the possible origin of the differences between our results and the previous ones, obtained on the same systems (the Gillette foams of [9, 23]) using the same experimental displays. First, Da Cruz *et al.* [9] report a 200 s^{-1} preshear; we observe that applying such high shear rate to the Gillette NR foam with the geometry used in [9] leads to expelling a large amount of the material from the gap by inertial forces (this happens for shear rates higher than 30 s^{-1}); therefore the protocol was inappropriate, leading to incorrect rheological data. Then the yield stress reported is $\approx$180 Pa, a value much higher than values reported in the literature [14, 27, 31]. This would mean that the material on which the measurements were performed in [9] was not what it was supposed to be. The case of the Rodts *et al.* data [23] is less obvious. They report a 7 Pa yield stress, which is lower than data from the literature [14, 27, 31]. Such a low value may indicate a material that is wetter than it should be, yet it is unclear why this would lead to shear banding.

It was recently shown that some non-shear-banding materials may exhibit transient shear banding [16] when a low velocity is applied after a short resting period; this is not observed when the low velocity is applied just after a high velocity. In order to check that the observations of Rodts *et al.* were not due to such a transient effect, we have studied the role of the shear history. MRI velocity measurements were performed under various conditions, when going from high to low velocities, from low to high velocities, and when rotating directly after a long resting time: all procedures were found to provide the same velocity profiles, *i.e.* no shear banding (even transient) was observed. The occurrence of shear banding in [23] might be due to uncontrolled traces of impurities in the system, e.g. clay particles, which were also studied with the same equipment. It was indeed shown that tiny amounts of colloidal clay particles dispersed in the continuous phase of a simple emulsion could form bridges between droplets and lead to thixotropic effects and shear banding [32]; the same might happen with a foam. Finally, let us stress that we provide here a consistent set of data performed with five different foams, including the Gillette foams of [9,23], with two different experiments. The conclusion is the absence of observable shear banding in all the foams we studied.

We now compare our upper bounds on $\dot{\gamma}_c$ with the model of Denkov *et al.* [24] (Eq. 1). Fig. 1c shows these bounds vs. the bubble radius for SLES foam ($\phi = 92\%$) as well as the $\dot{\gamma}_c$ value reported in [23]. It also shows the data obtained by Denkov *et al.* with foams of the same surfactants as in SLES foam mixed with myristic acid. Note that these last data were obtained in a 8 to 15 bubbles-wide gap, a case where finite size effects may be observed [20]. When the timescale of shear $1/\dot{\gamma}$ is lower than the duration of bubble rearrangements, there may be stress heterogeneities at the bubble scale, leading to shear banding in a thin layer [33], which is not bulk shear banding.

There is a strong discrepancy between the model and our data; the model overestimates the critical shear rate $\dot{\gamma}_c$ for all the studied foams, as shown in Tab. 1. This means that, while the proposed mechanism in [24] is certainly relevant in some cases, it may not apply to the foams made from ionic surfactant solutions without salt addition that are used in this study. Liquid films actually thin until the balance between capillary and disjoining pressures is reached, and form equilibrium common black films of thickness in the range 10-100 nm rather than very thin Newton black films. Moreover, the model assumes rigid interfaces, which sets the boundary conditions of the film thinning flow profile. However mobile interfaces, as in SLES foam, should lead to faster thinning, and thus to even higher critical shear rate than with rigid interfaces. This qualitative argument shows that the interfacial rigidity cannot account for the difference between the experimental upper bound of $\dot{\gamma}_c$ and Eq. 1. More experiments, in systems with strong attraction between the films, are needed to further test the model.

Nevertheless, as noted in the introduction, the absence of shear banding in foams is consistent with the basic mechanisms that tune shear banding in other complex fluids [3]. In particular, it is consistent with observations in dense emulsions [13].

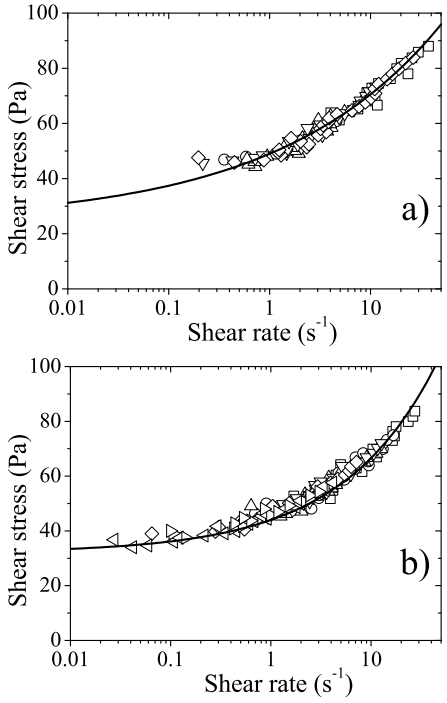

Fig. 3: Local constitutive laws measurements of a) Gillette NR foam ($\langle d \rangle = 41\,\mu$m), and b) SLES foam ($\phi = 92\%$, $\langle d \rangle = 45\,\mu$m). Each symbol corresponds to local measurements performed at a same rotational velocity. The solid lines are Herschel-Bulkley fits to the data $\tau = \tau_y + \eta_{HB}\dot{\gamma}^n$, with $\tau_y = 24$Pa, $\eta_{HB} = 25$Pa.s^n, $n = 0.27$ for the Gillette NR foam, $\tau_y = 32$Pa, $\eta_{HB} = 12$Pa.s^n, $n = 0.46$ for the SLES foam.

Constitutive law – The constitutive laws accounting for the materials' velocity profiles can be built from our experimental data. From the torque measurements T and the stress balance equations, one gets the shear stress distribution in the gap $\tau(R) = T/(2\pi H R^2)$. The local shear rate $\dot{\gamma}(R)$ in the gap is inferred from the velocity profiles $V(R)$ through $\dot{\gamma}(R) = V/R - \mathrm{d}V/\mathrm{d}R$. Both measurements performed at a given radius R for a given rotational velocity Ω thus provide a data point of the local constitutive law. We checked that the materials remain homogeneous unpon shear, which allows us to combine the data measured at various radii. The local constitutive laws $\tau(\dot{\gamma})$ obtained for two of the studied foams are plotted in Fig. 3a and 3b.

We find that the local flows curves obtained from experiments performed at various Ω are consistent with a single – local – constitutive law for each foam. This contrasts with recent results in 2D sheared foams [20] where no single local constitutive law can account for flow profiles obtained at different Ω. The same difference – non-local and local constitutive laws – is observed with emulsions flows

in microchannels [22] or in our wide gap Couette geometry [13]. As in [13, 22], the main difference between our observations and those of Katgert *et al.* [20] may stand in the bubble size to gap ratio (*i.e.* nonlocal effects are finite size effects). The gap of our geometry is indeed about 500 bubbles wide, whereas the gaps used in [20] are 20 to 40 bubbles wide. Leaving these possible finite size effects apart, it can finally be concluded that foams, together with emulsions [13] and Carbopol gels [12], belong to the class of simple yield stress fluids [3].

The local constitutive laws we obtain are well fitted to Herschel-Bulkley laws, with exponents consistent with those of foams with rigid (n=0.27) or mobile (n=0.46) interfaces [28]. We also remark that the Herschel-Bulkley consistency η_{HB} of the SLES foam is in fair agreement with the Denkov *et al.* prediction (see Eq. 5 of [28]). Note finally that, due to the limited range of low strain rates measurements, the yield stress for Gillette NR foam is probably underestimated

Conclusion – Our measurements demonstrate that three-dimensional foams do not exhibit observable signatures of shear banding, in contrast with previous observations [9, 23]. The question remains open whether steady shear banding may occur in extremely dry foams since it has been observed upon shear start-up [26]. Our results disagree with the recent model of Denkov *et al.* [24], which is shown here to overestimate the critical shear rate – if any – of the foams we studied. Further experiments with strong attraction between films would be needed to test the mechanism proposed in [24]. While nonlocal effects have been recently evidenced [20], we have finally shown that the constitutive law of foams measured locally in a wide gap geometry is that of simple Herschel-Bulkley yield stress fluids, as emulsions [13] and Carbopol gels [12]. Experiments at both small and large scales on a same system, as in of Goyon *et al.* [22], remain to be performed to test the non-local modelling of 3D foam flows.

* * *

We thank P. Coussot and S. Rodts for providing their data and for open discussions on their papers. We also thank R. Höhler and N. Denkov for fruitful discussions, and H. Sizun for crucial technical help. We gratefully acknowledge financial support from E.S.A. (MAP No. AO99-108: C14914/02/NL/SH).

REFERENCES

[1] Liu A. J. and Nagel S. R. (Editors), *Jamming and Rheology: Constrained Dynamics on Microscopic and Macroscopic Scales* (Taylor & Francis, New York) 2001.
[2] Dennin M., *J. Phys. Condens. Matter*, **20** (2008) 283103.
[3] Ovarlez G., Rodts S., Chateau X. and Coussot P., *Rheol. Acta*, **48** (2009) 831.
[4] Schall P. and van Hecke M., *Annu. Rev. Fluid Mech.*, **42** (2010) 67.
[5] Coussot P., Raynaud J. S., Bertrand F., Moucheront P., Guilbaud J. P., Huynh H. T., Jarny S. and Lesueur D., *Phys. Rev. Lett.*, **88** (2002) 218301.
[6] Møller P. C. F., Rodts S., Michels M. A. J. and Bonn D., *Phys. Rev. E*, **77** (2008) 041507.
[7] Manneville S., *Rheol. Acta*, **47** (2008) 301.
[8] Coussot P., Nguyen Q. D., Huynh H. T. and Bonn D., *Phys. Rev. Lett.*, **88** (2002) 175501.
[9] Da Cruz F., Chevoir F., Bonn D. and Coussot P., *Phys. Rev. E*, **66** (2002) 051305.
[10] Rogers S. A., Vlassopoulos D. and Callaghan P. T., *Phys. Rev. Lett.*, **100** (2008) 128304.
[11] Fall A., Bertrand F., Ovarlez G. and Bonn D., *Phys. Rev. Lett.*, **103** (2009) 178301.
[12] Coussot P., Tocquer L., Lanos C. and Ovarlez G., *J. Non-Newtonian Fluid Mech.*, **158** (2009) 85.
[13] Ovarlez G., Rodts S., Coussot P., Goyon J. and Colin A., *Phys. Rev. E*, **78** (2008) 036307.
[14] Höhler R. and Cohen-Addad S., *J. Phys.: Condens. Matter*, **17** (2005) R1041.
[15] Bécu L., Manneville S. and Colin A., *Phys. Rev. Lett.*, **96** (2006) 138302.
[16] Divoux T., Tamarii D., Barentin C. and Manneville S., *Phys. Rev. Lett.*, **104** (2010) 208301.
[17] Wang Y., Krishan K. and Dennin M., *Phys. Rev. E*, **73** (2006) 031401.
[18] Janiaud E., Weaire D. and Hutzler S., *Phys. Rev. Lett.*, **97** (2006) 038302.
[19] Krishan K. and Dennin M., *Phys. Rev. E*, **78** (2008) 051504.
[20] Katgert G., Tighe B. P., Möbius M. E. and van Hecke M., *Europhys. Lett.*, **90** (2010) 54002.
[21] Gilbreth C., Sullivan S. and Dennin M., *Phys. Rev. E*, **74** (2006) 051406.
[22] Goyon J., Colin A., Ovarlez G., Ajdari A. and Bocquet L., *Nature*, **454** (2008) 84.
[23] Rodts S., Baudez J. C. and Coussot P., *Europhys. Lett.*, **69** (2005) 636.
[24] Denkov D., Tcholakova S., Golemanov K. and Lips A., *Phys. Rev. Lett.*, **103** (2009) 118302.
[25] Krishan K., Helal A., Höhler R. and Cohen-Addad S., *Phys. Rev. E*, **82** (2010) 011405.
[26] Rouyer F., Cohen-Addad S., Vignes-Adler M. and Höhler R., *Phys. Rev. E*, **67** (2003) 021405.
[27] Gopal A. D. and Durian D. J., *Journal of Colloid and Interface Science*, **213** (1999) 169.
[28] Denkov N.D., Tcholakova S., Golemanov K., Ananthpadmanabhan K.P. and Lips A., *Soft Matter*, **5** (2009) 3389.
[29] Rodts S., Bertrand F., Jarny S., Poullain P. and Moucheront P., *C. R. Chim.*, **7** (2004) 275.
[30] Ovarlez G., Bertrand F. and Rodts S., *J. Rheol.*, **50** (2006) 259.
[31] Rouyer F., Cohen-Addad S. and Höhler R., *Colloids Surf. A*, **263** (2005) 111.
[32] Ragouilliaux A., Ovarlez G., Shahidzadeh-Bonn N., Herzhaft B., Palermo T. and Coussot P., *Phys. Rev. E*, **76** (2007) 051408.
[33] Kabla A., Scheibert J. and Debregeas G., *J. Fluid Mech.*, **587** (2007) 45.